HHS Public Access

Author manuscript

ACS Sens. Author manuscript; available in PMC 2024 December 22.

Published in final edited form as:

ACS Sens. 2023 December 22; 8(12): 4636–4645. doi:10.1021/acssensors.3c01625.

Cancer Cell Targeting, Magnetic Sorting, and SERS Detection through Cell Surface Receptors

David Rist[1], **Tom DePalma**[3], **Emerie Stagner**[3], **Miranda M Tallman**[4], **Monica Venere**[2,4], **Aleksander Skardal**[2,3], **Zachary D. Schultz**[1,2,*]

[1]Department of Chemistry and Biochemistry, The Ohio State University, Columbus, Ohio 43210, United States

[2]The James Comprehensive Cancer Center, The Ohio State University, Columbus, Ohio 43210, United States

[3]Department of Biomedical Engineering, The Ohio State University, Columbus, Ohio 43210, United States

[4]Department of Radiation Oncology, The Ohio State University, Columbus, Ohio 43210, United States

Abstract

Integrins are cellular surface receptors responsible for activation of many cellular pathways in cancer. These integrin proteins can be specifically targeted by small peptide sequences that offer the potential for the differentiation of cellular subpopulations using magnetically assisted cellular sorting techniques. By adding a gold shell to the magnetic nanoparticles, these integrin-peptide interactions can be differentiated by surface enhanced Raman spectroscopy (SERS) providing a quick reliable method for on target binding. In this paper we demonstrate the ability to differentiate the peptide-protein interactions of the small peptides CDPGYIGSR and Cyclic RGDfC functionalized on gold coated magnetic nanoparticles with the integrins they are known to bind to using their SERS signal. SW480 and SW620 colorectal cancer cells known to have the integrins of interest were then magnetically sorted using these functionalized nanoparticles suggesting differentiation between the sorted populations and integrin populations among the 2 cell lines.

Graphical Abstract

*corresponding author: schultz.133@osu.edu.

Supporting Information Available: The following files are available free of charge. Cancer Cell Targeting, Magnetic Sorting, and SERS Detection through Cell Surface Receptors SI: The inclusion of thresholding data, complete Pearson correlation and model determination are discussed.

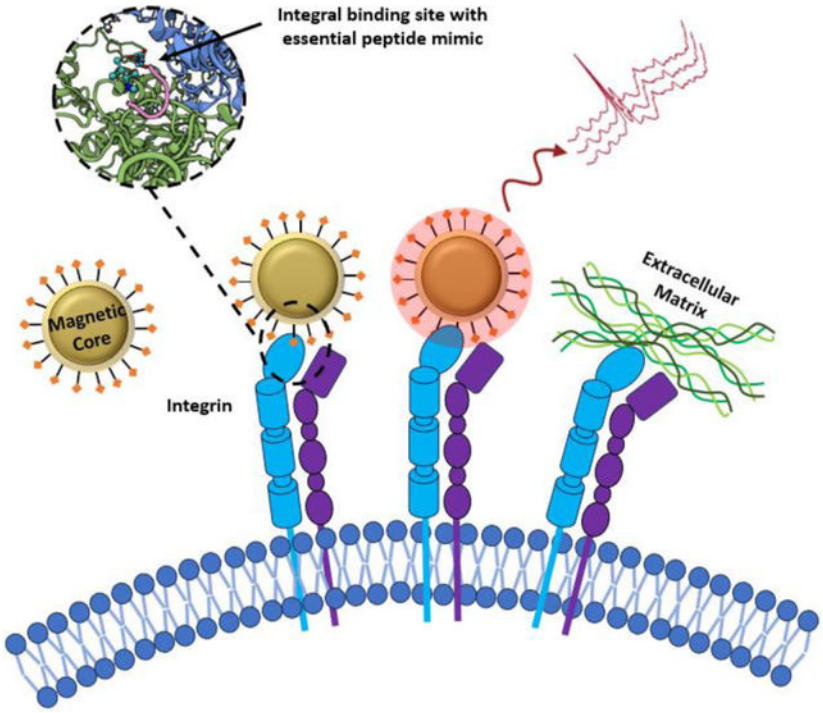

Keywords

Biosensor; Cancer; Peptide and Protein; Magnetic Sorting; Receptors; SERS

The formation of heterogeneous tumors is believed to have significant impact on treatment efficacy in cancer. As one example, glioblastoma (GBM) is a heterogeneous tumor believed to have at least 4 cellular subtypes, making it difficult to treat and characterize.[1] Likewise, in other cancer types, such as colorectal cancer, subpopulations can be stratified in a number of ways, including by accrual of mutations such as *WNT*, *KRAS* and *BRAF*, which can result in changes in proliferation and invasion potential. In cancer, attachment to, and detachment from, the extracellular matrix (ECM) regulates cellular signaling and invasiveness of the tumor.[2] The ECM consists of matrix molecules with which cellular receptor proteins interact to influence cellular signaling pathways, such as migration, maturation, differentiation, survival, and tissue homeostasis.[3] Since the ECM can regulate cellular differentiation, studying the ECM-cell interactions offers a potentially useful tool for differentiating tumor subpopulations allowing for more targeted treatments.

Three important and prominent structural components of the ECM are vitronectin, fibronectin and laminin, which bind cancer cells through integrin proteins and signal the activation of cellular pathways.[2–6] Integrins are a family of cellular surface receptors that mediate the attachment of cells to the ECM and have specificity in their binding based on the combination of α and β domains.[7] In order to target specific integrins and their interactions with the ECM, small peptides such as the Arg-Gly-Asp (RGD) and Tyr-Ile-Gly-Ser-Arg (YIGSR) can mimic vitronectin or fibronectin and laminin respectively.[8–11] The RGD peptide sequence targets two integrins, integrin $\alpha_v\beta_3$ and integrin $\alpha_5\beta_1$, that are

correlated with disease progression.[12–15] Integrin $\alpha_v\beta_3$ is associated with enhanced cellular motility and migration and resistance to apoptosis[12,16], while integrin $\alpha_5\beta_1$ is important in assembling the fibronectin matrix and initiating the cellular attachment to the ECM.[17] The YIGSR sequence on the other hand has been shown to bind to the β_1 integrin domain, specifically to the integrin $\alpha_6\beta_1$ but also has been reported to bind to integrin $\alpha_4\beta_1$.[18–20]

While these small peptide mimics have been used in cell spreading experiments[10,21] and to provide cell attachment points in 3D hydrogel cultures, their ability to be grafted or functionalized onto nanoparticles make them ideal probes for studying integrin binding to a given cancer cellular population. Raman probes[22] or fluorescent tags[23] are often used in conjunction with cellular imaging to assess a cell's binding phenotype. These methods provide intense signals, but with the loss of the chemical information at the binding site that is useful for analyzing specificity of the binding and the ability to differentiate the possible interactions. SERS is a nondestructive spectroscopic technique that is insensitive to water making it useful for studying biological systems[24] It has been shown previously that the RGD peptide has been functionalized onto gold nano-stars and the unique spectral fingerprint has allowed for label free identification of the proteins.[25,26]

In order to further enhance the signal, many studies have focused on changing the shape[27–29] or size[29] of the nanoparticles to selectively tune the localized surface plasmon resonance (LSPR) for the highest enhancement. Recently, there has been a growing interest in magnetic nanoparticles as SERS sensors with their ability to magnetically isolate the target of choice from complex media.[30] Magnetic nanoparticles can help further enhance SERS by inducing aggregation, generating hot spots between particles where coupled plasmon resonance can produce enhancements of around 10^{12}.[31–33]

In situ, the magnetic ability to remove them from complex media is helpful. However, there are even more exciting prospects *in situ*. Magnetic cellular sorting traditionally involves the use of antibodies to specifically target cells or to deplete a heterogeneous cellular population. This concept can be adapted by replacing antibodies with the small peptide mimics targeting specific integrin proteins expressed in the cell to selectively select for high integrin expression.

In this paper, we demonstrate the ability to differentiate integrins based on their spectral fingerprint. SERS spectra were acquired from Au-coated magnetic nanoparticles functionalized with CDPGYIGSR and cyclic-RGDfC and incubated with purified integrins $\alpha_4\beta_1$, $\alpha_5\beta_1$, $\alpha_6\beta_1$ and $\alpha_v\beta_3$. These SERS spectra were analyzed using multivariate curve resolution (MCR) to identify the characteristic spectra of each interaction. Furthermore, the confusion matrix for off target interactions was also acquired and compared to the MCR model to ensure signal contributed from off target interactions is insignificant and distinguishable from on target interactions. We show the ability to distinguish the peptide-protein interactions for 4 integrins that are essential in the process of cellular binding to the ECM. SW480 and SW620 colorectal cancer cell lines were then sorted using both CDPGYIGSR and Cyclic RGDfC functionalized gold coated magnetic nanoparticles to analyze the ability of the particles to select cellular subpopulations.

Experimental

Chemicals

Absolute Mag gold coated magnetic nanoparticles (capped with citrate, 250 nm diameter) were purchased from CD Bioparticles. Cyclic Arg – Gly - Asp -D – Phe – Cys (RGDfC), ≥95% was purchased from Biosynth. L-Cysteinyl-L-α-aspartyl-L-prolylglycyl-L-tyrosyl-L-isoleucylglycyl-L-seryl-N5-(diaminomethylene)-L-ornithine (CDPGYIGSR) ≥95% was purchased from ThermoFisher Scientific. Recombinant human Integrin $\alpha_v\beta_3$ ≥90%, Recombinant Human Integrin $\alpha_4\beta_1$ Protein, CF ≥90%, Recombinant Human Integrin $\alpha_5\beta_1$ Protein, CF ≥90% and Recombinant Human Integrin $\alpha_6\beta_1$, CF ≥95% were purchased from R&D systems. Ultrapure water from a Thermo Scientific GenPure UB-TOC/UF xCAD water purification system was used. Magnesium chloride ($MgCl_2$) and calcium chloride ($CaCl_2$) were purchased from Sigma Aldrich and phosphate buffered saline (PBS) was bought from Gibco Life Technologies Corporation. RPMI Medium was purchased from ThermoFischer Scientific. Fetal Bovine Serum one shots were purchased from Gibco. SW480 and SW620 cell lines were purchased from American Type Cell Culture (ATCC, Manassas, VA, USA) and validated using STR sequencing. All chemicals were used without further purification.

Instrumentation

SERS measurements were performed on an InVia Qontor Renishaw microscope using a 633 nm laser and 50X long working distance objective (0.5 NA). Zetasizer measurements were recorded using a Malvern Zetasizer ZS. Extinction measurements were performed on a Cary 4000 UV Vis instrument. Nanoparticle Tracking Analysis was performed on a Nanosight NS300. An Accumet Basic AB 15 pH probe was used for pH measurements.

Peptide Functionalization of Gold Coated Magnetic Nanoparticles

To functionalize peptide onto the nanoparticles, 100 μL of gold coated magnetic nanoparticles (1.54×10^{10} nanoparticles/mL) were centrifuged at 7000 relative centrifugal force (rcf) for 15 minutes and the supernatant was removed. To the particles, 630 μL of ultrapure water was added along with 70 μL of stock peptide (1 mM CDPGYIGSR or 1.15 mM Cyclic RGDfC). Particles were then allowed to shake overnight in Eppendorf tubes encapsulated in foil to ensure no photo damage of the nanoparticles occurred. After shaking overnight, the functionalized nanoparticles were centrifuged at 7000 rcf for 15 minutes and the supernatant was removed. The particles were washed with 700 μL of ultrapure water to ensure excess peptide was removed. Particles were resuspended in 1 mL of ultrapure water and the extinction was measured from 200–800 nm. The zeta potential of the peptide functionalized nanoparticles was then recorded at pH ≈ 6 and after adjustment using 0.1 M HCl to reach pH ≈ 4. Particles were again centrifuged as before, and the supernatant was removed before they were resuspended in 200 μL of ultrapure water and sonicated for about 5 minutes to ensure a stable suspension. 5 μL of each peptide nanoparticle suspension was then dropped onto a glass slide and allowed to dry while under an external magnetic force from the bottom of the slide. Raman measurements were then taken using a Renishaw InVia microscope with a 633 nm laser, 0.14 mW of power and 1 second acquisition times.

Incubation of Integrin Proteins with Peptide functionalized nanoparticles

Once the gold coated magnetic nanoparticles were functionalized with peptides and characterized, the particles were centrifuged and resuspended in 100 μL of 10% Ca^{2+} and Mg^{2+} positive PBS except for Cyclic RGDfC with Integrin $\alpha_v\beta_3$ which was kept in water.

For CDPGYIGSR functionalized nanoparticles, four 50 μL aliquots of nanoparticle suspensions were separately incubated with 373 nM integrin $\alpha_4\beta_1$, 375 nM integrin $\alpha_5\beta_1$, 373 nM integrin $\alpha_v\beta_3$, and 347 nM integrin $\alpha_6\beta_1$, respectively, for 2 hours while shaking. From this solution 5 μL were dropped onto a glass slide while under an external magnetic field and dried in air prior to (SERS) measurements.

Protein treatment of cyclic RGDfC functionalized nanoparticles followed a similar procedure. Four different 50 μL aliquots of particles were incubated with 373 nM integrin $\alpha_4\beta_1$, 375 nM integrin $\alpha_5\beta_1$,217 nM integrin $\alpha_v\beta_3$, and 347 nM integrin $\alpha_6\beta_1$ respectively for 2 hours. The same procedure was used for acquiring SERS spectra.

Cell Passage and Sorting

Human SW620 and SW480 colon cancer cells derived from commercial cell lines (ATCC) were passaged at approximately 80% confluency in 1640 RPMI medium supplemented with 10% Fetal Bovine Serum. The cells were cultured in tissue culture plates at about 80% confluency at 37°C with a 5% CO_2 humidified atmosphere. Trypsin with EDTA was then added to the flask for 5 minutes to cause detachment from the plate but to maintain viability of the cells prior to recovery and incubation. After passage, cells were allowed to recover their surface markers by sitting for 2 hours with a slight rock in a conical vial every 30 minutes in 10% FBS medium. Afterwards cells were resuspended in 500 μL of DPBS with $CaCl_2$ and $MgCl_2$. Cells were then counted using a 5-fold trypan blue in a Fuchs Rosenthal hemocytometer to determine the number of cells. Enough particles functionalized with peptide also resuspended in DPBS with $CaCl_2$ and $MgCl_2$ were to constitute 40 particles/cell and allowed to incubate for 2 hours with the cells with rocking every 30 minutes. The cells were then counted using a 2-fold dilution with trypan blue to ensure suspension. The cells were then centrifuged for 5 minutes at 300 rcf and the cells were resuspended in 2 mL of EasySep Sorting buffer and allowed to magnetically separate for 5 minutes using an EasySep cell separation magnet. The supernatant was saved as the not magnetically separated (negative) cell concentration. While 2 mL of sorting buffer was used to rinse off the magnetically separated (positive). Each population was once again centrifuged for 5 minutes at 300 rcf and resuspended in 500 μL of DPBS with $CaCl_2$ and $MgCl_2$. Each population was then once again recounted using a 2-fold dilution with Trypan Blue.

SERS Mapping of Cells

Sorted SW620 and SW480, positive and negative subpopulations, were allowed to adhere overnight in 10% FBS 1640 RPMI medium on glass cover slips. Cells were then fixed with 4% paraformaldehyde for 15 minutes before being washed with water prior to imaging. Raman maps were then taken on a Qontor Renishaw InVia microscope with a 633 nm laser, 0.37 mW of power, 50X long working distance objective (0.5 NA) and 1 second acquisition times.

Data Analysis

MATLAB R2020b was used for all data analysis. Raman spectra from peptides and their interactions with integrin proteins were baseline corrected using adaptive iteratively reweighted penalized least squares (airPLS).[34] Spectra were then integrated for total intensity. The standard deviation of the peaks showing consistent low integrated intensity was obtained and a threshold of three times the standard deviation plus the mean of these points were used to set a threshold for spectra that showed signal. The data was reduced to only the spectra that showed any signal above this set threshold (Figures S3–S4). All spectra kept were then normalized to their most intense peak. To reduce *the* dimensionality of the data, multivariate curve resolution alternating least squares (MCR-ALS) was performed using the PLS Toolbox in MATLAB. The normalized spectra were used without further preprocessing. Raman cell maps for the sorted populations were baselined corrected and Pearson correlation scores were calculated for each expected interaction compared to the MCR loadings generated.

Results and Discussion

Peptide Characterization

Gold coated magnetic nanospheres were functionalized with extracellular matrix (ECM) peptide mimics to investigate their corresponding SERS spectrum when incubated with integrin proteins. For the well-studied fibronectin motif of Arg-Gly-Asp (RGD), cyclic Arg-Gly-Asp-Phe-Cys (RGDfC) has been used previously for similar integrin binding studies.[26,35,36] Figure 1A shows SERS spectra normalized to the most intense peak of cyclic RGDfC functionalized nanoparticles compared to the unfunctionalized citrate capped nanoparticles. The functionalized cyclic RGDfC nanoparticles exhibit a characteristic peak at 1003 cm^{-1} and 1030 cm^{-1} attributed to phenylalanine, which is not present in stock citrate capped nanoparticles.[37,38] Bare particles exhibit a peak at 997 cm^{-1} that is spectroscopically distinct from the phenylalanine peaks observed once the peptide was functionalized. Large standard deviations as shown in the shaded area (Figure 1A) can be explained by the forced aggregation and generation of hot spots from pulling the nanoparticles with a magnet to a spot. While this forced aggregation generates more potential hot spots for increased SERS enhancement, the variable distance between particles can cause the overall intensity to fluctuate drastically.[39]

Laminin can be mimicked using the peptide motif of Tyr–Ile–Gly-Ser–Arg (YIGSR). To ensure specific integrin binding and provide thiol chemistry for easy functionalization, the peptide Cys–Asp–Pro –Gly–Tyr-Ile-Gly-Ser-Arg (CDPGYIGSR) was used for its ability to promote cell attachment[10,19]. Unlike the RGD peptide motif, there are no readily assigned peaks from peptide on the nanoparticles as shown in Figure 1B. However, the change in spectral background from the bare implies a change on the surface of the nanoparticles.

Successful functionalization of the peptide to the nanoparticles was confirmed by complimentary methods. Due to the weak acid/base nature of the amino acids, changes in the overall peptide charge can occur as the pH of the solution changes. Thus, the surface charge of the functionalized particles should be responsive to pH, whereas bare particles'

surface charge is less responsive. Zeta potential was measured right after functionalization (pH around 6) and following pH adjustment to 4. These pH's spans the isoelectric points of the peptides on the particles, 5.4 for Cyclic RGDfC and 5.9 for CDPGYIGSR., respectively. The change in the zeta potential for the cyclic RGDfC functionalzied nanoparticles is smaller than the CDPGYIGSR peptide, an observation that can be attributed to the cyclic nature of the RGDfC peptide which increases the peptide's resistance to pH changes.[40]

Statistically significant changes ($p < 0.01$) in the surface charge are seen when the peptide functionalized particles are functionalized and when they are protonated at the lower pH compared to the bare citrate capped nanoparticles (Figure 2). Furthermore, for functionalization of particles with both cyclic RGDfC and CDPGYIGSR, a slight plasmon shift from 608 nm to 610 nm is observed and a slight increase in absorbance from the peptide backbone is seen at 205 nm.[41] (Figure S1).

Protein Incubation

It has been previously shown that the interaction between integrin proteins and their corresponding ligands can be studied by analyzing their Raman signals.[26,35,36,42] By utilizing the plasmonic features of the gold coated magnetic nanoparticles, a SERS enhancement of the binding site of the ligand-protein interaction can be observed. Extracellular matrix components, and thus peptide mimics, are known to bind to multiple different integrins. This leads to the potential for multiple binding partners on a cell for a given peptide. SERS offers the ability to quickly determine which interaction is occurring, providing information about expression of integrin proteins in a given cell line. This label free approach offers a significant advantage over the commonly performed approaches due to its unique spectral specificity. Figure 3A shows the SERS signals of peptide functionalized nanoparticles with different integrin receptors the attached peptide is known to bind with. The SERS spectra and standard deviations of the known on-target peptide-integrin interactions[11,12,17,18,43–46] and reported interactions (CDPGYIGSR – Integrin $\alpha_4\beta_1$)[19] (Figure 3A) offer not only evidence of binding, as a labeled approach does, but also chemical information about the binding site of the interaction. Standard deviations in Figure 3A are also explained by the nature of hot spots,[39] with added uncertainty originating from the size and orientation of these proteins. Even with consistent binding, the portion of the protein in the hot spot might slightly differ, causing some variation in spectral signatures. Prior work shows that a model that characterizes the interaction with a pattern, or spectrum, best representative of that interaction can account for slight variance in the location of the protein relative to the hot spot.[26] To identify these spectral patterns, MCR was performed using a 4-component model and was determined sufficient for effectively separating the four unique interactions that were expected and explained 72.6% of the total variance. The loadings for the corresponding components as seen in Figure 3B strongly resemble the average SERS spectra of the average peptide-protein interactions. Additionally, as more components were loaded into the model, the variance explained did not substantially increase after 4 components (Figure S2)

Peptide-Protein Discrimination

Scores were generated using each unique peptide integrin binding set. Scores were then plotted in star coordinate plots.[47] Star coordinate plots, useful for two-dimensional representation of data greater than two dimensions, were used to visualize the specificity of each component to a specific interaction. These plots display data as a sum of vectors added together. Scores on component 1 were made to be the positive x component, while scores on component 3 were assigned to be negative x. Scores on component 2 were made to be the positive y component for the model, and component 4 were made to be the negative y component. This was to ensure similar peptides would be on opposite sides as to help ensure these components would not create confusion in the 2-dimensional space. The scores on all components were then added together, representing each acquired spectrum, to determine a 2-dimensional coordinate position.

Scores for each of the four interaction components from the model in Figure 3B are plotted along a unique vector. The cyclic RGDfC - integrin $\alpha_v\beta_3$ interaction was placed on the +x axis and to ensure specificity the cyclic RGDfC - integrin $\alpha_5\beta_1$ was placed on the -x axis of the star coordinate plot. The interactions of CDPGYIGSR with integrin $\alpha_6\beta_1$ (+y) and $\alpha_4\beta_1$ (-y) completed the coordinate axes.

To determine if the models could effectively be used to distinguish the integrins after they bound to the peptide, spectra from the peptide with and without integrins were scored on the model generated previously. As seen in Figure 4A, cyclic RGDfC functionalized particles when bound with integrins $\alpha_v\beta_3$ and $\alpha_5\beta_1$ nicely separate with most of the bound integrin $\alpha_v\beta_3$ scoring on component 1 and the bound integrin $\alpha_5\beta_1$ scoring along the axis of component 3. The particles in the absence of the integrin cluster near the origin. Some of the spread in this plot can be attributed to a slightly weaker binding signal or a low intensity hot spot. In Figure 4B, a similar behavior is observed for the CDPGYIGSR functionalized particles. While the CDPGYIGSR functionalized particles score near the origin in the absence of integrin, their interaction with integrin $\alpha_6\beta_1$ score on component 2 and integrin $\alpha_4\beta_1$ score on component 4. Some of the overlap present, especially between the Cyclic RGDfC – Integrin $\alpha_v\beta_3$ and CDPGYIGSR - integrin $\alpha_6\beta_1$ interactions, can be understood due to the lack of aromatic amino acids present in the CDPGYIGSR – integrin $\alpha_6\beta_1$ binding pocket and thus produces a less definitive SERS spectrum compared to the other interactions. This shows that SERS response can differentiate between different proteins binding to the peptides on the nanoparticles. This differentiation indicates SERS spectral data allows for the classification of the integrins without interference of the peptide confounding the signal, and despite the variance in hotspot formation and protein location within these hotspots.

To be able to correctly identify the interaction present in cells, as well as to ensure the specificity of the peptide -protein interactions, on-target interactions need to be distinguishable from each other. Using the same model as in Figure 3, a star coordinates plot was made for the 4 on target interactions (Figure 5A). Each targeted peptide-protein interaction scatters along a unique separate axis, indicating exclusivity from each other.

To ensure that there are no off-target signatures that would affect identification of the peptide-protein interaction, CDPGYIGSR was incubated with integrins $\alpha_v\beta_3$ and $\alpha_5\beta_1$ and cyclic RGDfC was incubated with integrins $\alpha_4\beta_1$ and $\alpha_6\beta_1$. As expected, Figure 5B shows that the scores from any off-target interactions that occur scatter randomly towards the center of the plotThis indicates poor scoring on all components of the model, and no consistent interaction. Most of the spectra taken of these off-target interactions showed no binding or spectral signal (Figure S5)

Spectral Analysis

By analyzing the structure of the RGD ligand with integrins $\alpha_v\beta_3$[48] and $\alpha_5\beta_1$[49], spectral assignments were made for the corresponding average SERS spectra. Strong Raman scattering aromatic amino acids such as tyrosine, tryptophan, and phenylalanine largely dominate these signals. For integrin $\alpha_5\beta_1$ peaks at 794 cm^{-1} (Tyr)[38], 1368[38] and 1616 cm^{-1} (Tyr, Trp)[37,38,50] largely dominate the signal. For integrin $\alpha_v\beta_3$ the peaks at 1001 cm^{-1} (Phe)[37,38], and 1597 cm^{-1} (Phe)[38] dominate. Analysis of the SERS corresponding cyclic RGD- integrin spectra was done by comparing them with their reported crystal structures[48,49].With the YIGSR peptide and its corresponding interaction being less studied, it was assumed that amino acids within or near the binding site are represented in the corresponding spectra.

Signals from the integrin binding events include peaks that are different than those of the peptides used to target the integrins. Peaks at 611 cm^{-1} (Cys, Arg. C-C Twisting)[38,51], 1360 cm^{-1} (Trp)[37,38,52,53], and 1642 cm^{-1} (Amide I)[52] dominate for the $\alpha_4\beta_1$ integrin binding. Meanwhile integrin $\alpha_6\beta_1$ shows fewer spectral features although peaks at 1453 cm^{-1} (C-H bending in proteins)[54] and 1575 cm^{-1} (Trp, His) are present[38,55]. Full peak assignments for the resulting average spectra of each peptide-protein interaction are included in Tables S1–S4.

Cellular Sorting

SW480 and SW620 are commonly used colorectal cancer cell lines that have been well studied in literature and have previously been shown to express binding to Cyclic RGDfC[35,36]. Using the peptide functionalized magnetic nanoparticles. It was found that for Cyclic RGDfC, the percentage of sorted cells were 16.8 ± 6.5% and 11.0 ± 4.0% for SW480 and SW620 cell populations respectively as shown in Figure 6A. Previous literature reports that SW480 cells have been shown to express more of the α_v subunit than the SW620 cell line while both have comparable β_3 expression.[56] Also, it is has been previously reported that SW480 cells have shown higher expression when bound with a CD44+ antibody which has been shown to have a direct connection the Integrin $\alpha_5\beta_1$.[57,58] The differences observed based on peptide interaction based sorting are not statistically significant at the 95% confidence level. Furthermore, when these populations were instead incubated with CDPGYIGSR particles, the percentage of sorted cells 17.1 ± 4.9% and 12.7 ± 4.3% for SW480 and SW620 cells respectively as shown in Figure 6B. SW480 cells are reported to have equivalent α_6 expression[56,57,59] but increased β_1 expression.[56,59] Our results indicate the observed differences in the sorting of SW480 from SW620 cells are again not statistically significant. This is different from what was expected prior to the sort

as the integrin expression for these two cell lines is reported to be different.[56] However, the fact that a population is being sorted suggests that the sort might be based on more than just the presence of the integrin protein, and that there might be some underlying biology that could be explored further.

Dark field images and Raman maps were taken for each sorted population of cells fixed with 4% paraformaldehyde. The Pearson correlation coefficient was calculated for each pixel in the map comparing the observed spectra to the generated MCR components. Figure 7 shows the Pearson correlation map for MCR component 1 and one of the highly correlated spots from a positively sorted SW620 cell with the Cyclic RGDfC peptide functionalized nanoparticles. When this component is compared to a cell from the negatively sorted population, there appears to be no particles present and thus confirming no binding to the cell as expected. Only the positive cells seem to show any correlation or presence of particles, indicating a binding event occurs. Visual comparison of the spectrum (Figure 7C) shows the agreement with the MCR component associated with the binding interaction. To ensure there were no other off-target interactions, Pearson correlation maps were generated for the positive and negative sorted cells against each MCR component from off-target integrins (Figure S6–S7). Similarly, for the cyclic RGDfC sorted cells, the SW620 cell line Raman maps show differences in binding between the positive and negative cell populations when sorted with the CDPGYIGSR functionalized nanoparticles (Figure 8). The Raman maps with the CDPGYIGSR functionalized nanoparticles also correlate to the expected interactions as previously discussed, indicating that the SERS spectrum can be used to differentiate the binding responsible for different peptide-based cell sorting (Figure S8–S9). Maps were also taken of the SW480 cell line and show similar binding behavior to the SW620 cell line. Again, negative and positive sort populations can be differentiated by the expected binding interactions (Figure S10–S13). It should be noted unbound particles were also present on both the slides for the positive and negative populations suggesting the number of particles used per cell was in excess and not limiting. Continued investigations may further elucidate differences in receptor expression that regulates the differences in cellular populations sorted and the underlying biology of the sorted populations.

Conclusion

In conclusion, gold coated magnetic nanoparticles were functionalized with ECM peptide mimics (cyclic RGDfC and CDPGYIGSR), to act as biorecognition agents for specific integrin proteins. SERS, zeta potential, and extinction measurements confirm functionalization of the peptides onto the nanoparticles. The functionalized nanoparticles were then incubated with various integrins that would be present in a cell in situ. Corresponding label free SERS signals were then shown to be specific and were used to differentiate between on-target interactions as well as showing nonspecific binding from off-target interactions. The developed probe and corresponding signals will be useful in potential cellular sorting of heterogeneous cell populations that interact with the extracellular matrix. This also provides a fast, nondestructive method for confirming the presence of integrins in a cellular population. Furthermore, cellular sorting was performed using both peptides on SW620 and SW480 cancer cells showing the particles may be useful for potential cellular sorting after further optimization.

Supplementary Material

Refer to Web version on PubMed Central for supplementary material.

Acknowledgment.

This work was supported by The Ohio State University and the National Institutes of Health Award R01 GM109988 (ZS), the President's Research Excellence (PRE) Accelerator Grant program (ZS, AS, MV), and The Ohio State University Comprehensive Cancer Center and the National Institutes of Health under grant number P30 CA016058.

References

(1). Verhaak RGW; Hoadley KA; Purdom E; Wang V; Qi Y; Wilkerson MD; Miller CR; Ding L; Golub T; Mesirov JP; Alexe G; Lawrence M; O'Kelly M; Tamayo P; Weir BA; Gabriel S; Winckler W; Gupta S; Jakkula L; Feiler HS; Hodgson JG; James CD; Sarkaria JN; Brennan C; Kahn A; Spellman PT; Wilson RK; Speed TP; Gray JW; Meyerson M; Getz G; Perou CM; Hayes DN; Cancer Genome Atlas Research Network. Integrated Genomic Analysis Identifies Clinically Relevant Subtypes of Glioblastoma Characterized by Abnormalities in PDGFRA, IDH1, EGFR, and NF1. Cancer Cell 2010, 17 (1), 98–110. 10.1016/j.ccr.2009.12.020. [PubMed: 20129251]

(2). Hatoum A; Mohammed R; Zakieh O The Unique Invasiveness of Glioblastoma and Possible Drug Targets on Extracellular Matrix. Cancer Manag Res 2019, 11, 1843–1855. 10.2147/CMAR.S186142. [PubMed: 30881112]

(3). Mohiuddin E; Wakimoto H Extracellular Matrix in Glioblastoma: Opportunities for Emerging Therapeutic Approaches. Am J Cancer Res 2021, 11 (8), 3742–3754. [PubMed: 34522446]

(4). Oomura A; Nakamura T; Arakawa M; Ooshima A; Isemura M Alterations in the Extracellular Matrix Components in Human Glomerular Diseases. Virchows Arch A Pathol Anat Histopathol 1989, 415 (2), 151–159. 10.1007/BF00784353. [PubMed: 2500770]

(5). Bachman H; Nicosia J; Dysart M; Barker TH Utilizing Fibronectin Integrin-Binding Specificity to Control Cellular Responses. Adv Wound Care (New Rochelle) 2015, 4 (8), 501–511. 10.1089/wound.2014.0621. [PubMed: 26244106]

(6). Belkin AM; Stepp MA Integrins as Receptors for Laminins. Microsc Res Tech 2000, 51 (3), 280–301. 10.1002/1097-0029(20001101)51:3<280::AID-JEMT7>3.0.CO;2-O. [PubMed: 11054877]

(7). Barczyk M; Carracedo S; Gullberg D Integrins. Cell Tissue Res 2010, 339 (1), 269–280. 10.1007/s00441-009-0834-6. [PubMed: 19693543]

(8). Boateng SY; Lateef SS; Mosley W; Hartman TJ; Hanley L; Russell B RGD and YIGSR Synthetic Peptides Facilitate Cellular Adhesion Identical to That of Laminin and Fibronectin but Alter the Physiology of Neonatal Cardiac Myocytes. American Journal of Physiology-Cell Physiology 2005, 288 (1), C30–C38. 10.1152/ajpcell.00199.2004. [PubMed: 15371257]

(9). Cheng S; Craig WS; Mullen D; Tschopp JF; Dixon D; Pierschbacher MD Design and Synthesis of Novel Cyclic RGD-Containing Peptides as Highly Potent and Selective Integrin .Alpha.IIb.Beta.3 Antagonists. J. Med. Chem 1994, 37 (1), 1–8. 10.1021/jm00027a001. [PubMed: 7507165]

(10). Massia SP; Rao SS; Hubbell JA Covalently Immobilized Laminin Peptide Tyr-Ile-Gly-Ser-Arg (YIGSR) Supports Cell Spreading and Co-Localization of the 67-Kilodalton Laminin Receptor with Alpha-Actinin and Vinculin. Journal of Biological Chemistry 1993, 268 (11), 8053–8059. 10.1016/S0021-9258(18)53062-3. [PubMed: 8463322]

(11). Yoshida N; Ishii E; Nomizu M; Yamada Y; Mohri S; Kinukawa N; Matsuzaki A; Oshima K; Hara T; Miyazaki S The Laminin-Derived Peptide YIGSR (Tyr–Ile–Gly–Ser–Arg) Inhibits Human Pre-B Leukaemic Cell Growth and Dissemination to Organs in SCID Mice. Br J Cancer 1999, 80 (12), 1898–1904. 10.1038/sj.bjc.6690618. [PubMed: 10471037]

(12). Danhier F; Le Breton A; Préat V RGD-Based Strategies To Target Alpha(v) Beta(3) Integrin in Cancer Therapy and Diagnosis. Mol. Pharmaceutics 2012, 9 (11), 2961–2973. 10.1021/mp3002733.

(13). Desgrosellier JS; Cheresh DA Integrins in Cancer: Biological Implications and Therapeutic Opportunities. Nat Rev Cancer 2010, 10 (1), 9–22. 10.1038/nrc2748. [PubMed: 20029421]

(14). Mao Y; Schwarzbauer JE Accessibility to the Fibronectin Synergy Site in a 3D Matrix Regulates Engagement of α 5β 1 versus α vβ 3 Integrin Receptors. Cell Communication & Adhesion 2006, 13 (5–6), 267–277. 10.1080/15419060601072215. [PubMed: 17162669]

(15). Bowditch RD; Hariharan M; Tominna EF; Smith JW; Yamada KM; Getzoff ED; Ginsberg MH Identification of a Novel Integrin Binding Site in Fibronectin. Differential Utilization by Beta 3 Integrins. Journal of Biological Chemistry 1994, 269 (14), 10856–10863. 10.1016/S0021-9258(17)34137-6. [PubMed: 7511609]

(16). Sheldrake HM; Patterson LH Function and Antagonism of Beta3 Integrins in the Development of Cancer Therapy. Curr Cancer Drug Targets 2009, 9 (4), 519–540. 10.2174/156800909788486713. [PubMed: 19519320]

(17). Koivunen E; Wang B; Ruoslahti E Isolation of a Highly Specific Ligand for the Alpha 5 Beta 1 Integrin from a Phage Display Library. J Cell Biol 1994, 124 (3), 373–380. 10.1083/jcb.124.3.373. [PubMed: 7507494]

(18). Sanchez-Esteban J; Wang Y; Filardo EJ; Rubin LP; Ingber DE Integrins B1, A6, and A3 Contribute to Mechanical Strain-Induced Differentiation of Fetal Lung Type II Epithelial Cells via Distinct Mechanisms. American Journal of Physiology-Lung Cellular and Molecular Physiology 2006, 290 (2), L343–L350. 10.1152/ajplung.00189.2005. [PubMed: 16169900]

(19). Cell-Adhesive Activity and Receptor-Binding Specificity of the Laminin-Derived YIGSR Sequence Grafted onto Staphylococcal Protein A1 | The Journal of Biochemistry | Oxford Academic. https://academic.oup.com/jb/article-abstract/115/2/182/768279?redirectedFrom=fulltext&login=false (accessed 2022-02-14).

(20). Schaff M; Tang C; Maurer E; Bourdon C; Receveur N; Eckly A; Hechler B; Arnold C; de Arcangelis A; Nieswandt B; Denis CV; Lefebvre O; Georges-Labouesse E; Gachet C; Lanza F; Mangin PH Integrin A6β1 Is the Main Receptor for Vascular Laminins and Plays a Role in Platelet Adhesion, Activation, and Arterial Thrombosis. Circulation 2013, 128 (5), 541–552. 10.1161/CIRCULATIONAHA.112.000799. [PubMed: 23797810]

(21). Yu C; Law JBK; Suryana M; Low HY; Sheetz MP Early Integrin Binding to Arg-Gly-Asp Peptide Activates Actin Polymerization and Contractile Movement That Stimulates Outward Translocation. Proceedings of the National Academy of Sciences 2011, 108 (51), 20585–20590. 10.1073/pnas.1109485108.

(22). Huang R; Harmsen S; Samii JM; Karabeber H; Pitter KL; Holland EC; Kircher MF High Precision Imaging of Microscopic Spread of Glioblastoma with a Targeted Ultrasensitive SERRS Molecular Imaging Probe. Theranostics 2016, 6 (8), 1075–1084. 10.7150/thno.13842. [PubMed: 27279902]

(23). Wu P-H; Onodera Y; Ichikawa Y; Rankin EB; Giaccia AJ; Watanabe Y; Qian W; Hashimoto T; Shirato H; Nam J-M Targeting Integrins with RGD-Conjugated Gold Nanoparticles in Radiotherapy Decreases the Invasive Activity of Breast Cancer Cells. IJN 2017, 12, 5069–5085. 10.2147/IJN.S137833. [PubMed: 28860745]

(24). Lai H; Xu F; Wang L A Review of the Preparation and Application of Magnetic Nanoparticles for Surface-Enhanced Raman Scattering. Journal of Materials Science 2018, 53 (12), 8677–8698. 10.1007/s10853-018-2095-9.

(25). Sloan-Dennison S; Bevins MR; Scarpitti BT; Sauvé VK; Schultz ZD Protein Corona-Resistant SERS Tags for Live Cell Detection of Integrin Receptors. Analyst 2019, 144 (18), 5538–5546. 10.1039/C9AN01056D. [PubMed: 31402356]

(26). Sloan-Dennison S; Schultz ZD Label-Free Plasmonic Nanostar Probes to Illuminate in Vitro Membrane Receptor Recognition. Chem. Sci 2019, 10 (6), 1807–1815. 10.1039/C8SC05035J. [PubMed: 30842849]

(27). Lu X; Rycenga M; Skrabalak SE; Wiley B; Xia Y Chemical Synthesis of Novel Plasmonic Nanoparticles. Annual Review of Physical Chemistry 2009, 60 (1), 167–192. 10.1146/annurev.physchem.040808.090434.

(28). Wu X; Xia Y; Huang Y; Li J; Ruan H; Chen T; Luo L; Shen Z; Wu A Improved SERS-Active Nanoparticles with Various Shapes for CTC Detection without Enrichment Process with Supersensitivity and High Specificity. ACS Appl. Mater. Interfaces 2016, 8 (31), 19928–19938. 10.1021/acsami.6b07205. [PubMed: 27434820]

(29). Guo P; Sikdar D; Huang X; Jye Si, K.; Xiong W; Gong S; Wei Yap, L.; Premaratne M; Cheng W Plasmonic Core–Shell Nanoparticles for SERS Detection of the Pesticide Thiram: Size- and Shape-Dependent Raman Enhancement. Nanoscale 2015, 7 (7), 2862–2868. 10.1039/C4NR06429A. [PubMed: 25599516]

(30). Donnelly T; Smith WE; Faulds K; Graham D Silver and Magnetic Nanoparticles for Sensitive DNA Detection by SERS. Chem. Commun 2014, 50 (85), 12907–12910. 10.1039/C4CC06335J.

(31). A Hybridization Model for the Plasmon Response of Complex Nanostructures | Science. https://www.science.org/doi/abs/10.1126/science.1089171 (accessed 2023-03-13).

(32). Probing the Structure of Single-Molecule Surface-Enhanced Raman Scattering Hot Spots | Journal of the American Chemical Society. https://pubs.acs.org/doi/10.1021/ja8051427 (accessed 2023-03-13).

(33). Futamata M Single Molecule Sensitivity in SERS: Importance of Junction of Adjacent Ag Nanoparticles. Faraday Discuss 2006, 132, 45–61; discussion 85–94. 10.1039/b506406f. [PubMed: 16833107]

(34). Zhang Z-M; Chen S; Liang Y-Z Baseline Correction Using Adaptive Iteratively Reweighted Penalized Least Squares. Analyst 2010, 135 (5), 1138–1146. 10.1039/b922045c. [PubMed: 20419267]

(35). Xiao L; Wang H; Schultz ZD Selective Detection of RGD-Integrin Binding in Cancer Cells Using Tip Enhanced Raman Scattering Microscopy. Anal. Chem 2016, 88 (12), 6547–6553. 10.1021/acs.analchem.6b01344. [PubMed: 27189228]

(36). Wang H; Schultz ZD TERS Detection of αVβ3 Integrins in Intact Cell Membranes. ChemPhysChem 2014, 15 (18), 3944–3949. 10.1002/cphc.201402466. [PubMed: 25212599]

(37). Cheng W-T; Liu M-T; Liu H-N; Lin S-Y Micro-Raman Spectroscopy Used to Identify and Grade Human Skin Pilomatrixoma. Microscopy Research and Technique 2005, 68 (2), 75–79. 10.1002/jemt.20229. [PubMed: 16228983]

(38). Zhu G; Zhu X; Fan Q; Wan X Raman Spectra of Amino Acids and Their Aqueous Solutions. Spectrochimica Acta Part A: Molecular and Biomolecular Spectroscopy 2011, 78 (3), 1187–1195. 10.1016/j.saa.2010.12.079. [PubMed: 21242101]

(39). Sergiienko S; Moor K; Gudun K; Yelemessova Z; Bukasov R Nanoparticle–Nanoparticle vs. Nanoparticle–Substrate Hot Spot Contributions to the SERS Signal: Studying Raman Labelled Monomers, Dimers and Trimers. Physical Chemistry Chemical Physics 2017, 19 (6), 4478–4487. 10.1039/C6CP08254H. [PubMed: 28120963]

(40). Ji X; Nielsen AL; Heinis C Cyclic Peptides for Drug Development. Angewandte Chemie International Edition n/a (n/a), e202308251. 10.1002/anie.202308251.

(41). Anthis NJ; Clore GM Sequence-Specific Determination of Protein and Peptide Concentrations by Absorbance at 205 Nm. Protein Sci 2013, 22 (6), 851–858. 10.1002/pro.2253. [PubMed: 23526461]

(42). Chowdhury MH; Gant VA; Trache A; Baldwin AM; Meininger GA; Coté GL Use of Surface-Enhanced Raman Spectroscopy for the Detection of Human Integrins. JBO 2006, 11 (2), 024004. 10.1117/1.2187022. [PubMed: 16674194]

(43). Kapp TG; Rechenmacher F; Neubauer S; Maltsev OV; Cavalcanti-Adam EA; Zarka R; Reuning U; Notni J; Wester H-J; Mas-Moruno C; Spatz J; Geiger B; Kessler H A Comprehensive Evaluation of the Activity and Selectivity Profile of Ligands for RGD-Binding Integrins. Sci Rep 2017, 7 (1), 39805. 10.1038/srep39805. [PubMed: 28074920]

(44). Haubner R; Gratias R; Diefenbach B; Goodman SL; Jonczyk A; Kessler H Structural and Functional Aspects of RGD-Containing Cyclic Pentapeptides as Highly Potent and Selective Integrin αVβ3 Antagonists. J. Am. Chem. Soc 1996, 118 (32), 7461–7472. 10.1021/ja9603721.

(45). Liu S Radiolabeled Multimeric Cyclic RGD Peptides as Integrin Avβ3 Targeted Radiotracers for Tumor Imaging. Mol. Pharmaceutics 2006, 3 (5), 472–487. 10.1021/mp060049x.

(46). Frith JE; Mills RJ; Hudson JE; Cooper-White JJ Tailored Integrin–Extracellular Matrix Interactions to Direct Human Mesenchymal Stem Cell Differentiation. Stem Cells Dev 2012, 21 (13), 2442–2456. 10.1089/scd.2011.0615. [PubMed: 22455378]

(47). Kandogan E; Road H; Jose S Star Coordinates: A Multi-Dimensional Visualization Technique with Uniform Treatment of Dimensions

(48). Xiong J-P; Stehle T; Zhang R; Joachimiak A; Frech M; Goodman SL; Arnaout MA Crystal Structure of the Extracellular Segment of Integrin αVβ3 in Complex with an Arg-Gly-Asp Ligand. Science 2002, 296 (5565), 151–155. 10.1126/science.1069040. [PubMed: 11884718]

(49). Nagae M; Re S; Mihara E; Nogi T; Sugita Y; Takagi J Crystal Structure of A5β1 Integrin Ectodomain: Atomic Details of the Fibronectin Receptor. Journal of Cell Biology 2012, 197 (1), 131–140. 10.1083/jcb.201111077. [PubMed: 22451694]

(50). Stone N; Kendall C; Shepherd N; Crow P; Barr H Near-Infrared Raman Spectroscopy for the Classification of Epithelial Pre-Cancers and Cancers. Journal of Raman Spectroscopy 2002, 33 (7), 564–573. 10.1002/jrs.882.

(51). Chan JW; Taylor DS; Zwerdling T; Lane SM; Ihara K; Huser T Micro-Raman Spectroscopy Detects Individual Neoplastic and Normal Hematopoietic Cells. Biophysical Journal 2006, 90 (2), 648–656. 10.1529/biophysj.105.066761. [PubMed: 16239327]

(52). Stone N; Kendall C; Smith J; Crow P; Barr H Raman Spectroscopy for Identification of Epithelial Cancers. Faraday Discuss 2004, 126 (0), 141–157. 10.1039/B304992B. [PubMed: 14992404]

(53). Li X; Yang T; Li S; Yu T Surface-Enhanced Raman Spectroscopy Differences of Saliva between Lung Cancer Patients and Normal People. In Clinical and Biomedical Spectroscopy and Imaging II (2011), paper 808722; Optica Publishing Group, 2011; p 808722. 10.1364/ECBO.2011.808722.

(54). Nogueira GV; Jr LSS; Martin AA; Zângaro RA; Pacheco MTT; M.d, C MC; M.d, P CA Raman Spectroscopy Study of Atherosclerosis in Human Carotid Artery. JBO 2005, 10 (3), 031117. 10.1117/1.1908129. [PubMed: 16229642]

(55). Madzharova F; Heiner Z; Kneipp J Surface Enhanced Hyper-Raman Scattering of the Amino Acids Tryptophan, Histidine, Phenylalanine, and Tyrosine. J. Phys. Chem. C 2017, 121 (2), 1235–1242. 10.1021/acs.jpcc.6b10905.

(56). Schlaeppi M; Rüegg C; Traň-Thang C; Chapuis G; Tevaearai H; Lahm H; Sordat B Role of Integrins and Evidence for Two Distinct Mechanisms Mediating Human Colorectal Carcinoma Cell Interaction with Peritoneal Mesothelial Cells and Extracellular Matrix. Cell Adhesion and Communication 1997, 4 (6), 439–455. 10.3109/15419069709004460. [PubMed: 9177905]

(57). Slater C; De La Mare J-A; Edkins AL In Vitro Analysis of Putative Cancer Stem Cell Populations and Chemosensitivity in the SW480 and SW620 Colon Cancer Metastasis Model. Oncol Lett 2018, 15 (6), 8516–8526. 10.3892/ol.2018.8431. [PubMed: 29805588]

(58). McFarlane S; McFarlane C; Montgomery N; Hill A; Waugh DJJ CD44-Mediated Activation of A5β1-Integrin, Cortactin and Paxillin Signaling Underpins Adhesion of Basal-like Breast Cancer Cells to Endothelium and Fibronectin-Enriched Matrices. Oncotarget 2015, 6 (34), 36762–36773. [PubMed: 26447611]

(59). Comparative evaluation of integrin α- and β-chain expression in colorectal carcinoma cell lines and in their tumours of origin | SpringerLink https://link.springer.com/article/10.1007/BF00196144 (accessed 2023-03-08).

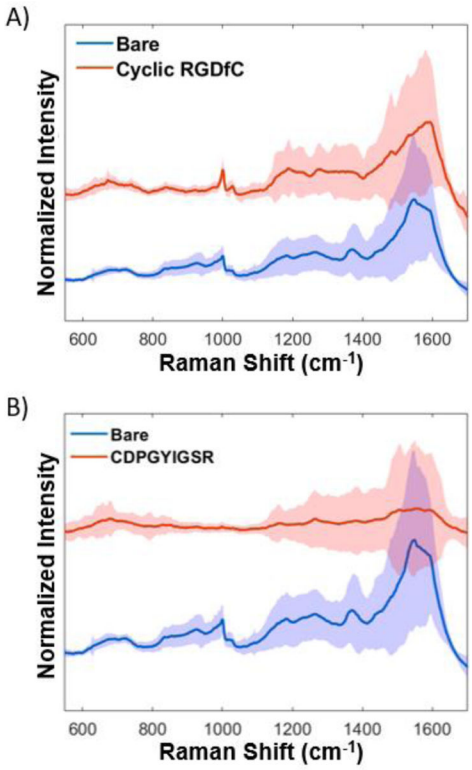

Figure 1.

(A) Average SERS signals from baselined and normalized SERS spectra of Au nanoparticles and Cyclic RGDfC nanoparticles with shaded standard deviations (B) Average SERS signals from baselined and normalized SERS spectra of Au nanoparticles and CDPGYIGSR nanoparticles with shaded standard. Spectra were normalized to the most intense peak.

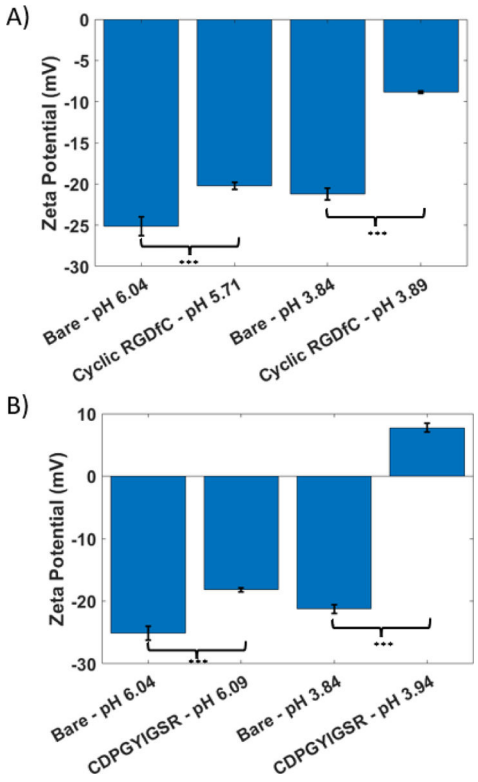

Figure 2:

(A) Zeta potential measurements of bare and cyclic RGDfC functionalized nanoparticles above and below the isoelectric point of the peptide (B) Zeta potential measurements of bare and CDPGYIGSR nanoparticles above and below the isoelectric point of the peptide. *** denotes p-value < 0.01.

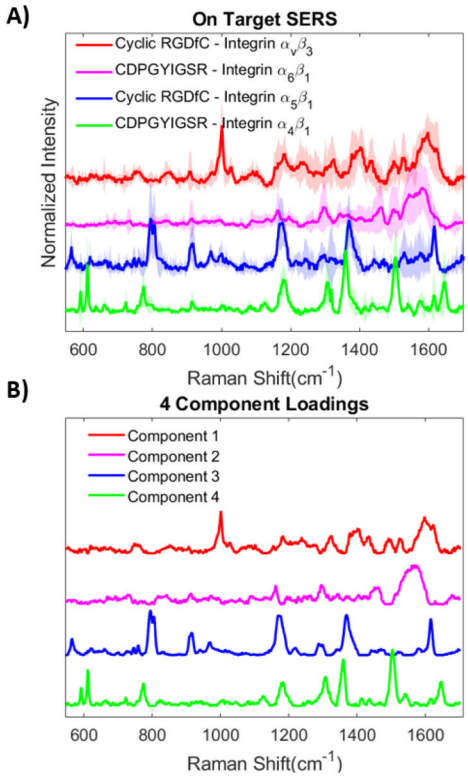

Figure 3.

(A) Normalized and average SERS spectra with standard deviations of Au nanoparticles functionalized with cyclo – RGDfC - Integrin $\alpha_v\beta_3$, cyclo – RGDfC - Integrin $\alpha_5\beta_1$, CDPGYIGSR - Integrin $\alpha_4\beta_1$ and CDPGYIGSR- Integrin $\alpha_6\beta_1$ and shaded standard deviations (B) Loadings for 4 component MCR model generated from peptide protein interaction on nanoparticles.

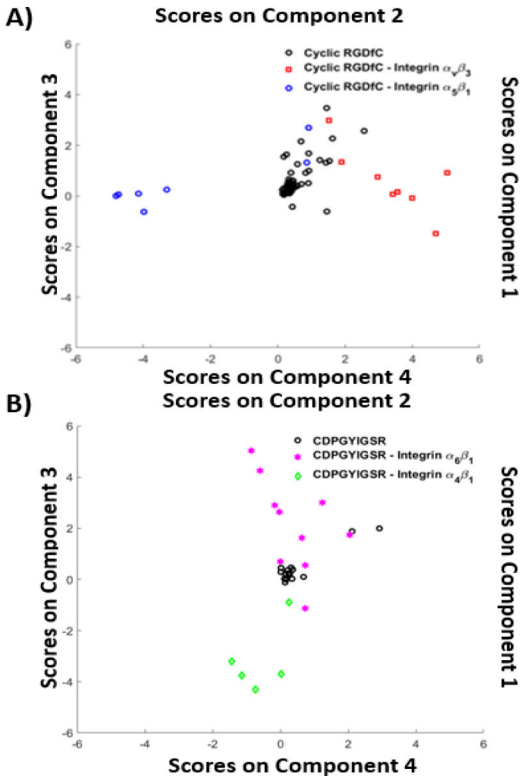

Figure 4.

(A) Star coordinates plot of expected Integrin interactions with component 1 scores set at +X, component 2 scores set as +y, component 3 scores set as –x and component 4 scores set as –y for cyclic RGDfC. (B) Star coordinates plot for CDPGYIGSR and expected binding integrins.

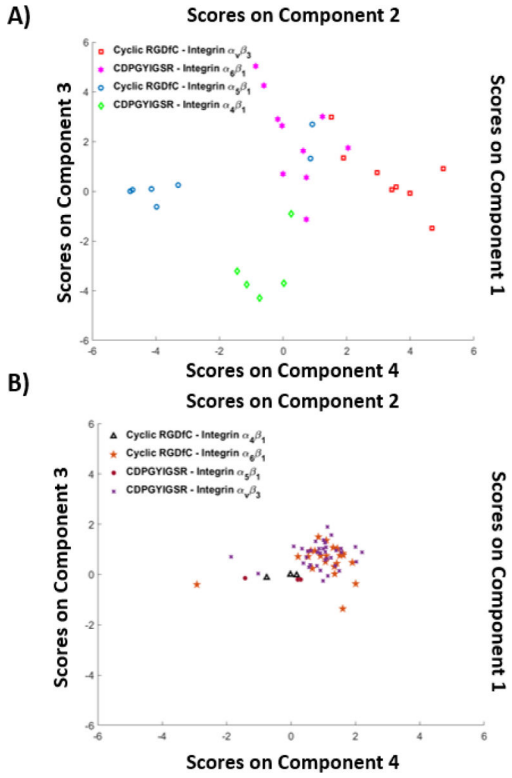

Figure 5.

(A) Star Coordinates plot of expected Integrin interactions with component 1 scores set at +X, component 2 scores set as +y, component 3 scores set as –x and component 4 scores set as –y. (B) Star coordinates plot for all off target interactions with peptides and integrins

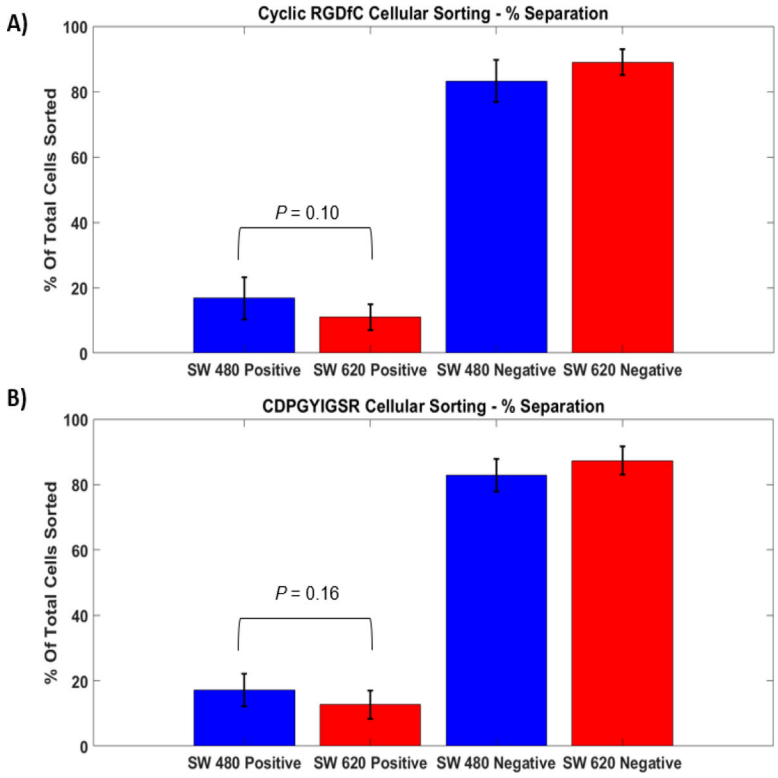

Figure 6.

(A) Percentage of cells sorted of SW480 (n=5) and SW620 (n=6) colorectal cancer cells with standard deviation bars using Cyclic RGDfC functionalized nanoparticles. (B) Percentage of SW480 (n = 4) and SW620 (n=7) colorectal cancer cells sorted with CDPGYIGSR functionalized nanoparticles.

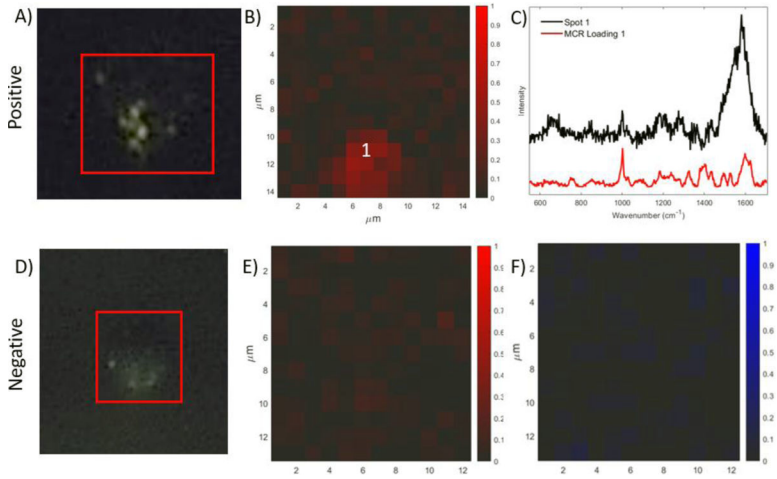

Figure 7.

A) Dark field image of a positively sorted SW620 cell with Cyclic RGDfC peptide functionalized nanoparticles. B) Pearson Correlation Map for Cyclic RGDfC – Integrin $\alpha_v\beta_3$ assigned component in the positively sorted cell. C) Spectra from a high scoring spot on the Pearson Correlation map. D) Dark field image of a negatively sorted SW620 cell with Cyclic RGDfC peptide functionalize nanoparticles. E) Pearson Correlation Map for Cyclic RGDfC – Integrin $\alpha_v\beta_3$ assigned component in the negatively sorted cell. F) Pearson Correlation Map for Cyclic RGDfC – Integrin $\alpha_5\beta_1$ assigned component in the negatively sorted cell.

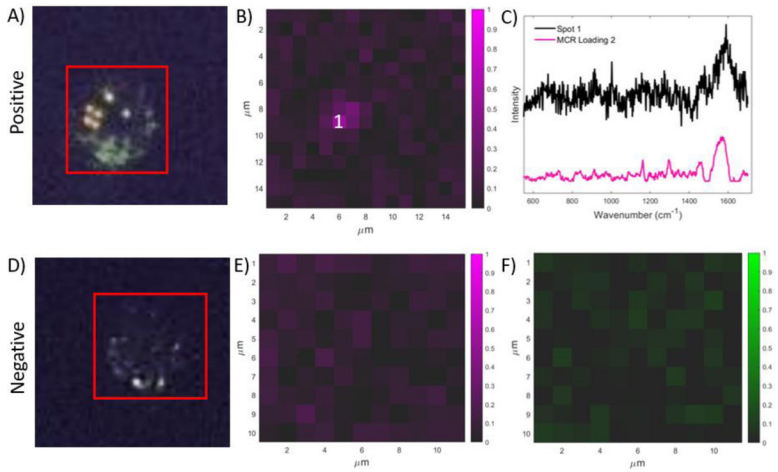

Figure 8.

A) Dark field image of a positively sorted SW620 cell with CDPGYIGSR peptide functionalized nanoparticles. B) Pearson Correlation Map for CDPGYIGSR – Integrin $\alpha_6\beta_1$ assigned component in the positively sorted cell. C) Spectrum from a high scoring point in the Pearson Correlation map. D) Dark field image of a negatively sorted SW620 cell with CDPGYIGSR peptide functionalized nanoparticles. E) Pearson Correlation Map for CDPGYIGSR – Integrin $\alpha_6\beta_1$ assigned component in the negatively sorted cell. F) Pearson Correlation Map for CDPGYIGSR – Integrin $\alpha_4\beta_1$ assigned component in the negatively sorted cell.